Cellular/Molecular

Permeant Ion Effects on External Mg^{2+} Block of NR1/2D NMDA Receptors

Anqi Qian and Jon W. Johnson
Department of Neuroscience, University of Pittsburgh, Pittsburgh, Pennsylvania 15260

Voltage-dependent channel block by external Mg^{2+} (Mg_o^{2+}) of NMDA receptors is an essential determinant of synaptic function. The resulting Mg_o^{2+} inhibition of NMDA responses depends strongly on receptor subunit composition: NR1/2A and NR1/2B receptors are more strongly inhibited by Mg_o^{2+} than are NR1/2C or NR1/2D receptors. Previous work showed that permeant ions have profound effects on Mg_o^{2+} block of NMDA receptors composed of NR1, NR2A, and NR2B subunits. Whether permeant ions affect Mg_o^{2+} inhibition of NR1/2C or NR1/2D receptors is unknown. We investigated the effects of permeant ions on Mg_o^{2+} block of NR1/2D receptors by integrating results from whole-cell recordings, single-channel recordings, and kinetic modeling. Lowering internal [Cs^+] caused a voltage-dependent decrease in the Mg_o^{2+} IC_{50} and in the apparent Mg_o^{2+} unblocking rate, and increase in the apparent Mg_o^{2+} blocking rate ($k_{+,app}$) of NR1/2D receptors. Lowering external [Na^+] caused modest voltage-dependent changes in the Mg_o^{2+} IC_{50} and $k_{+,app}$. These data can be explained by a kinetic model in which occupation of either of two external permeant ion binding sites prevents Mg_o^{2+} entry into the channel. Occupation of an internal permeant ion binding site prevents Mg_o^{2+} permeation and accelerates Mg_o^{2+} unblock to the external solution. We conclude that variations in permeant ion site properties shape the NR2 subunit dependence of Mg_o^{2+} block. Furthermore, the external channel entrance varies little among NMDA receptor subtypes. Differences in the Mg_o^{2+} blocking site, and particularly in the selectivity filter and internal channel entrance, are principally responsible for the subunit dependence of Mg_o^{2+} block.

Key words: **NMDA receptors; glutamate receptors; channel block; single channel; magnesium; inhibition**

Introduction

The NMDA subtypes of the ionotropic glutamate receptor family are widely distributed in the vertebrate CNS, exhibit unusual biophysical properties, and are broadly involved in CNS physiology (Dingledine et al., 1999; Lisman and McIntyre, 2001; Nakazawa et al., 2002). Functional NMDA receptors generally contain NR1 and NR2 subunits. There are four NR2 subunits (NR2A–NR2D) that follow distinct developmental and regional expression patterns. NMDA receptors are modulated via many mechanisms that display NR2 subunit specificity (Cull-Candy and Leszkiewicz, 2004).

Voltage-dependent channel block by Mg_o^{2+} is an essential NMDA receptor property. Investigation of Mg_o^{2+} block has improved understanding of synaptic regulation, mechanisms of drug action, and channel structure and gating. Mg_o^{2+} inhibition of NMDA receptors varies with brain region and developmental stage because of differential NR2 subunit expression coupled with NR2 subunit dependence of Mg_o^{2+} inhibition (Kato and Yoshimura, 1993; Monyer et al., 1994; Kuner et al., 1996; Momiyama et al., 1996; Qian et al., 2005).

The degree and voltage dependence of Mg_o^{2+} inhibition are powerfully modulated by permeant ions (Antonov and Johnson, 1999; Zhu and Auerbach, 2001a,b; Qian et al., 2002). Along with its mechanistic importance, permeant ion modulation of Mg_o^{2+} inhibition is likely to participate in nervous system physiology and pathology. Permeant ion concentration changes during synaptic transmission (Rose and Konnerth, 2001) are large enough to significantly modify Mg_o^{2+} inhibition. Much greater changes in permeant ion concentrations occur in pathological states (Grisar, 1984; Lux et al., 1986; Kager et al., 2000), and Mg_o^{2+} inhibition is altered by nervous system pathology, including nerve injury, inflammation, and chemical ischemia (Hori and Carpenter, 1994; Zhang et al., 1996; Aizenman et al., 2000; Furukawa et al., 2000; Guo and Huang, 2001). Changes in permeant ion concentration likely act in concert with other modulatory mechanisms (Chen and Huang, 1992; Zhang et al., 1996; Guo and Huang, 2001) to alter Mg_o^{2+} inhibition in pathological states.

Permeant ion effects on Mg_o^{2+} inhibition have been investigated for NMDA receptors that contain NR2A or NR2B subunits (Antonov and Johnson, 1999; Zhu and Auerbach, 2001a,b; Qian et al., 2002), but not for receptors that contain NR2C or NR2D subunits. Understanding permeant ion effects on Mg_o^{2+} inhibition of NR1/2D receptors, which play important physiological roles developmentally and in adults (Okabe et al., 1998; Bengzon et al., 1999; Hrabetova et al., 2000; Miyamoto et al., 2002; Thompson et al., 2002), would deepen insight into blocking

Received Aug. 9, 2006; revised Sept. 7, 2006; accepted Sept. 8, 2006.

This work was supported by National Institute of Mental Health Grants MH45817 and MH00944 (J.W.J.) and Predoctoral National Research Service Award MH12476 (A.Q.). We thank Richard Clarke and Beth Siegler for helpful comments on this manuscript.

Correspondence should be addressed to Jon W. Johnson, Department of Neuroscience, A410 Langley Hall, University of Pittsburgh, Pittsburgh, PA 15260. E-mail: johnson@bns.pitt.edu.

A. Qian's present address: Carnegie Mellon University in Qatar, 5032 Forbes Avenue, Quatar SMC 1070, Pittsburgh, PA 15289.

DOI:10.1523/JNEUROSCI.3453-06.2006

 0270-6474/06/2610899-12$15.00/0

mechanisms and their variation among NMDA receptor subtypes. We previously reported (Qian et al., 2005) that Mg_o^{2+} inhibits NR2A and NR2B subunit-containing NMDA receptors more effectively than NR1/2D receptors predominantly because Mg_o^{2+} unbinds more quickly from NR1/2D receptors. Here, we combined electrophysiological and modeling approaches to examine permeant ion effects on Mg_o^{2+} block of NR1/2D receptors. We found powerful permeant ion regulation mediated by binding to two external and one internal site (summarized in Fig. 7). Comparison of Mg_o^{2+} block models of NR1/2D and cortical receptors provides quantitative explanations for the NR2 subunit dependence of Mg_o^{2+} block.

Materials and Methods

Cell culture. Human embryonic kidney (HEK) 293T cells and HEK 293 cells (American Type Culture Collection, Manassas, VA) were used for whole-cell and outside-out patch recordings, respectively. The cells were cultured at 37°C in 5% CO_2/95% air in DMEM culture medium (Invitrogen, Carlsbad, CA) supplemented with 2 mM glutamine. Culture medium was supplemented with 5% fetal bovine serum (FBS) for 293T cells and with 10% FBS plus 1 mM sodium pyruvate for HEK 293 cells. Cells were split twice a week. For experiments, cells were plated onto glass coverslips pretreated with poly-D-lysine (0.1 mg/ml) and rat-tail collagen (0.1 mg/ml; BD Biosciences, San Jose, CA) at $1–4 \times 10^5$ cells per 35 mm dish.

Transfection. HEK 293 or 293T cells were transiently transfected 18–48 h after plating with cDNAs for rat NMDA receptor subunits (Buller and Monaghan, 1997): NR1-1a [GenBank accession number (GAN) X63255, in plasmid pcDM8] plus NR2A (GAN M91561, in plasmid pcDNA1) or NR2D (GAN L31612, in plasmid pcDM8). Enhanced green fluorescent protein (eGFP) cDNA was cotransfected as previously described (Qian et al., 2005). 293T cells were transfected using LipofectAMINE/PLUS reagents (Invitrogen) by adding to each dish 1 ml of serum-free medium containing 1 μg of total DNA (1 eGFP to 3 NR1 to 6 NR2A or 2D), 5 μl of LipofectAMINE, and 4 μl of PLUS. DL-APV (200 μM) was added to prevent NMDA receptor-mediated excitotoxicity. To transfect HEK 293 cells, we used a calcium phosphate precipitation procedure. A total of 2.8 μg of cDNA was used per dish (ratio of 1 eGFP to 1 NR1-1a to 2 NR2D). Precipitates were washed off with fresh culture medium plus 200 μM DL-APV 7–9 h after addition of DNA.

Solutions. Solutions were prepared and applied as previously described (Qian et al., 2002). NMDA receptors were activated by 10 or 30 μM NMDA plus 30 μM glycine. $MgCl_2$ was added to external solutions at the indicated concentrations with no adjustment of other solute concentrations. We used several solutions to test the effects of Na_o^+ and Cs_i^+ on Mg_o^{2+} block. The abbreviations and contents of external solutions are as follows (in mM): "140 Na_o^+" solution, 140 NaCl, 1 $CaCl_2$, 2.8 KCl, and 10 HEPES; "70 Na_o^+" solution, 70 NaCl, 140 sucrose, 0.5 $CaCl_2$, 2.8 KCl, and 10 HEPES. The abbreviations and contents of internal solutions are as follows (in mM): "125 Cs_i^+" solution for whole-cell experiments, 125 CsCl, 10 EGTA, and 10 HEPES; "125 Cs_i^+" solution for patch recordings, 115 CsF, 10 CsCl, 10 EGTA, and 10 HEPES; "8 Cs_i^+" solution for whole-cell experiments, 8 CsCl, 117 *N*-methyl-D-glucamine (NMDG), 10 EGTA, and 10 HEPES; "8 Cs_i^+" solution for patch recordings, 8 CsF, 117 NMDG, 10 EGTA, and 10 HEPES; "25 Cs_i^+" solution, 25 CsF, 100 NMDG, 10 EGTA, and 10 HEPES. Fluoride-based internal solutions were used for single-channel recordings to improve seal formation and stability of recordings (Marty and Neher, 1995). Osmolality and pH were adjusted as described previously (Qian et al., 2002). The junction potentials between the pipette and bath solution for internal/external solution combinations were as follows: 5 mV for 140 Na_o^+/125 Cs_i^+ (chloride-based); −3 mV for 140 Na_o^+/8 Cs_i^+ (chloride-based); −7 mV for 70 Na_o^+/8 Cs_i^+ (chloride-based); 9 mV for 140 Na_o^+/125 Cs_i^+ (fluoride-based), −3 mV for 140 Na_o^+/8 Cs_i^+ (fluoride-based), −7 mV for 70 Na_o^+/25 Cs_i^+ (fluoride-based). All membrane potentials reported here were corrected for junction potentials. Ultrapure salts were used when available. All chemicals were from Sigma (St. Louis, MO), except as indicated in the text.

Whole-cell recording and analysis. Whole-cell recordings were performed as previously described (Qian et al., 2002) 20–72 h after transfection. Briefly, currents were recorded at room temperature with an Axopatch 200A or 200B amplifier (Molecular Devices, Sunnyvale, CA), low-pass filtered at 10 kHz, and digitized at 44 kHz with a Neuro-Corder. Series resistance was compensated routinely (60–80%). NMDA-activated currents in the absence ($I_{control}$) and presence (I_{Mg}) of multiple $[Mg^{2+}]_o$ values were measured from −115 to −15 mV at 10 mV increments. The IC_{50} of Mg_o^{2+} at each voltage was estimated by fitting $I_{Mg}/I_{control}$ at various $[Mg^{2+}]_o$ values using Equation 1:

$$I_{Mg}/I_{control}\,(\%) = 100\%/[1 + ([Mg^{2+}]_o/IC_{50})^{n_H}]. \quad (1)$$

IC_{50} and n_H (Hill coefficient) were left as free parameters during fitting. Curve fitting was performed using Origin 4.0 or 6.0 (Microcal Software, Northampton, MA). The IC_{50} value at each voltage was derived from fits to $I_{Mg}/I_{control}$ measurements with three to six different $[Mg^{2+}]_o$ values and from 3 to 10 cells at each $[Mg^{2+}]_o$. At each voltage, Equation 1 was fit to each of the $I_{Mg}/I_{control}$ values pooled from all experiments, although for clarity only mean values ± SEM were plotted in Figure 1*C*. Error bars in Figures 1*D* and 2*C* show SE estimated during nonlinear curve fitting of Equation 1 by Origin.

Single-channel recording and analysis. Single-channel recording and analysis were performed as previously described (Qian et al., 2005). Outside-out patch recordings were performed at room temperature according to standard methods (Hamill et al., 1981). Pipettes (resistance, 5–8 MΩ) were pulled from borosilicate standard-wall glass with filaments (Warner Instrument, Portland, OR). Pipettes were coated with Sylgard and fire polished. Single-channel currents were recorded and stored on videotape for later analysis as described for whole-cell recording. Data were collected at voltages from −105 to −45 mV. At each voltage, single-channel currents in each patch were collected in segments of 50–240 s duration, with the first segment being a control measurement in 0 Mg_o^{2+}, followed by one to three additional segments in different $[Mg^{2+}]_o$ values. Data from at least three patches were used at each voltage.

For analysis, each recorded data segment was played back, filtered at 2.5 kHz (−3 dB; eight-pole, low-pass Bessel filter) and digitally sampled at 25 kHz using pCLAMP 8 (Molecular Devices). To optimize our ability to resolve brief events, we used the DC analysis programs (http://www.ucl.ac.uk/Pharmacology/dcpr95.html), which make use of time course fitting techniques (Colquhoun and Sigworth, 1995). Dwell time histograms were plotted on square root versus log time scales (Sigworth and Sine, 1987). A chosen time resolution (50 μs in most patches; range, 45–85 μs) was applied to dwell time distributions, and durations shorter than the value of the time resolution were deleted from both open- and closed-duration distributions. The resulting dwell time histograms were fitted by the maximum likelihood method (Colquhoun and Sigworth, 1995) and the value of the imposed time resolution was subtracted from the time constants of the fit.

Open-duration histograms in the absence or presence of Mg_o^{2+} were fit by one to three exponentials (see Fig. 4*B*), consistent with previous studies (Wyllie et al., 1996, 1998; Qian et al., 2005). The decrease of the time constant of the largest component (τ_o) with increasing $[Mg^{2+}]_o$ values was used to estimate Mg_o^{2+} blocking rate (see Results). We did not further characterize the other exponential components. Closed-duration histograms in the absence of Mg_o^{2+} were adequately fit by the sum of three or four exponentials (see Fig. 4*C*). In both the absence and presence of Mg_o^{2+}, closed duration histograms included the duration of all closures, regardless of the conductance level from which the closure began. In the presence of Mg_o^{2+}, an additional closed-duration component was observed (time constant, τ_b) in most experiments. This component was interpreted to represent blocking events by Mg_o^{2+} (Qian et al., 2005). Occasionally, when the value of τ_b was very close to the briefest closed-duration component observed in the absence of Mg_o^{2+}, the closed-duration histogram was fitted by the same number of exponentials in the absence and presence of Mg_o^{2+}. In those cases, the value of τ_b still could be estimated with reasonable accuracy because the time constant of the confounding brief closed-duration component was necessarily close to

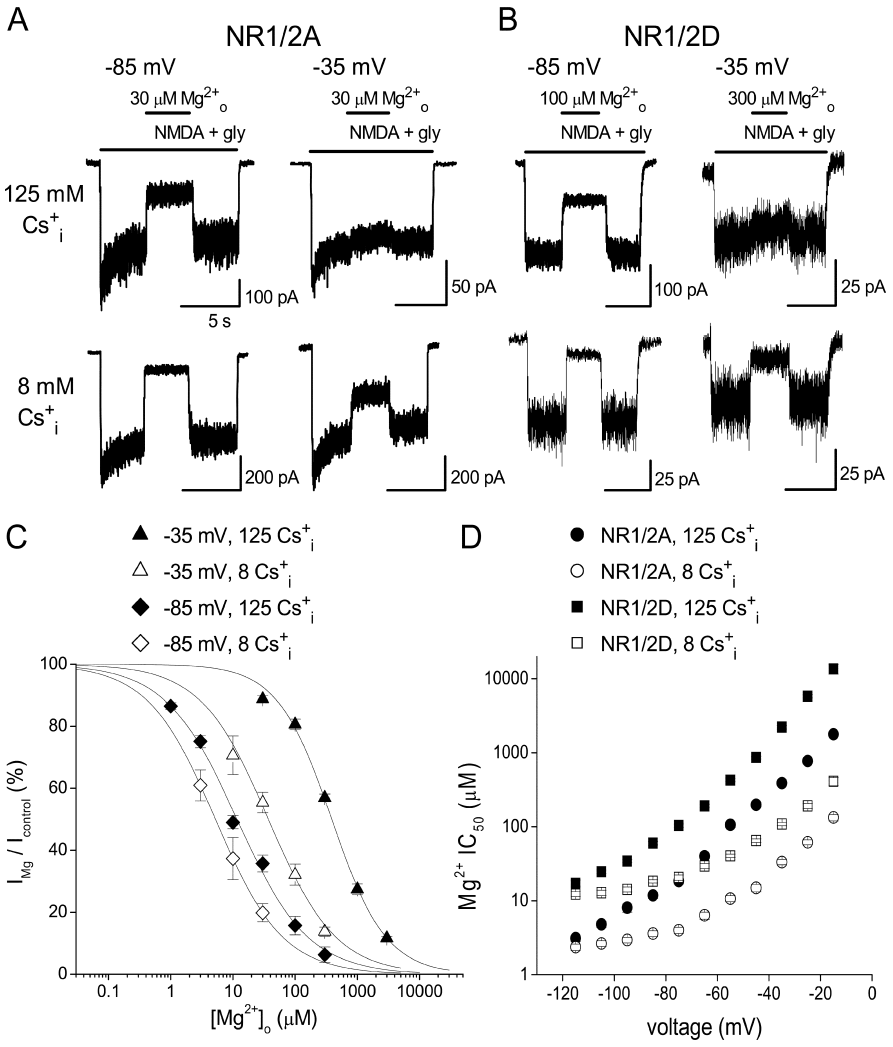

Figure 1. Effect of Cs_i^+ on Mg_o^{2+} inhibition of NMDA receptor whole-cell currents. ***A***, ***B***, Examples of inhibition by Mg_o^{2+} of NR1/2A (***A***) and NR1/2D (***B***) receptor currents in 140 Na_o^+/125 Cs_i^+ (top traces) and 140 Na_o^+/8 Cs_i^+ (bottom traces) solutions at the indicated voltages. The bars above the current traces indicate the time of drug application. At −85 mV and at −35 mV, Mg_o^{2+} inhibition of both NR1/2A and NR1/2D receptors was enhanced by lowering $[Cs^+]_i$. ***C***, Examples of concentration–inhibition curves for NR1/2A receptors in 140 mM Na_o^+; $[Cs^+]_i$ and voltage as indicated. The voltage, $[Cs^+]_i$, and Mg_o^{2+} IC_{50} values are as follows: −35 mV, 125 mM, 388 μM; −35 mV, 8 mM, 37.3 μM; −85 mV, 125 mM, 11.8 μM; −85 mV, 8 mM, 5.2 μM. Error bars indicate SEM. ***D***, Mg_o^{2+} IC_{50} values in 140 mM Na_o^+ are plotted from −115 to −15 mV; subunit combination and $[Cs^+]_i$ as indicated. Data in 140 Na_o^+/125 Cs_i^+ were replotted from Qian et al. (2005). Error bars indicate SE.

need for very high-quality recordings and the use of time course fitting in analysis made single-channel experiments extremely time-consuming. As a result, single-channel data were collected in only three ionic conditions. Adequate constraint of models was achieved by simultaneous fitting to single-channel and whole-cell experiments.

Results

Effect of changing $[Cs^+]_i$ and $[Na^+]_o$ on Mg_o^{2+} inhibition of whole-cell currents

We first characterized the effect of changing $[Cs^+]_i$ on Mg_o^{2+} inhibition of 293T whole-cell currents mediated by NR1/2A and NR1/2D receptors. Internal Cs^+ rather than K^+ was used so that data could be directly compared with previous results (Antonov et al., 1998; Antonov and Johnson, 1999; Qian et al., 2002, 2005); NMDA receptor permeabilities to Cs^+ and K^+ are nearly equal (Nowak et al., 1984; Tsuzuki et al., 1994). Mg_o^{2+} inhibited both NR1/2A and NR1/2D receptor responses more effectively in a lower $[Cs^+]_i$. For example, with NR1/2A receptors (Fig. 1*A*) at −85 mV, current inhibition by 30 μM Mg_o^{2+} was 1.3-fold greater in 140 Na_o^+/8 Cs_i^+ than in 140 Na_o^+/125 Cs_i^+. At −35 mV, current inhibition by 30 μM Mg_o^{2+} was 4.3-fold greater in 140 Na_o^+/8 Cs_i^+ than in 140 Na_o^+/125 Cs_i^+. With NR1/2D receptors (Fig. 1*B*), the effect of changing $[Cs^+]_i$ on Mg_o^{2+} inhibition was generally similar to that observed with NR1/2A receptors: lowering $[Cs^+]_i$ from 125 to 8 mM increased inhibition by 100 μM Mg_o^{2+} 1.4-fold at −85 mV and increased inhibition by 100 μM Mg_o^{2+} 4.9-fold at −35 mV.

To analyze the voltage dependence of the effect of $[Cs^+]_i$ on Mg_o^{2+} inhibition of NR1/2A and NR1/2D receptors, concentration–inhibition curves were constructed by measuring Mg_o^{2+} inhibition in multiple $[Mg^{2+}]_o$ values at each voltage (see Materials and Methods). Examples of these curves are shown in Figure 1*C* for NR1/2A receptors. At each voltage, concentration–inhibition curves are left-shifted in the lower $[Cs^+]_i$, indicating increased Mg_o^{2+} affinity. The shift was greater at −35 mV than at −85 mV. Figure 1*D* compares the voltage dependence of NR1/2A and NR1/2D receptor Mg_o^{2+} IC_{50} values over the range of voltages studied. It is clear that at any single voltage and $[Cs^+]_i$, Mg_o^{2+} IC_{50} was lower in NR1/2A than in NR1/2D receptors. For both receptors, lowering $[Cs^+]_i$ decreased Mg_o^{2+} IC_{50} and weakened its voltage dependence at hyperpolarized voltages.

The effects of changing $[Na^+]_o$ on Mg_o^{2+} inhibition of whole-cell currents of NR1/2A and NR1/2D receptors are illustrated in Figure 2. For these experiments, 8 mM Cs_i^+ was used in intracellular solutions to minimize the effect of Cs_i^+ on Mg_o^{2+} inhibition. Decreasing $[Na^+]_o$ from 140 to 70 mM moderately increased Mg_o^{2+} inhibition of NR1/2A receptors at both −105 and −45 mV (Fig. 2*A*). The same change in $[Na^+]_o$ slightly increased Mg_o^{2+} inhibition of NR1/2D receptors at −105 mV, but decreased

τ_b, and because the amplitude of the τ_b component was relatively large. We did not make corrections for missed events but estimated that they were not frequent under our experimental conditions (Qian et al., 2005).

The apparent Mg_o^{2+} blocking and unblocking rates, $k_{+,app}$ and $k_{-,app}$, were estimated as described in Neher and Steinbach (1978). The term "apparent" is used to distinguish from Mg_o^{2+} blocking and unblocking rates in the absence of permeant ion effect (Antonov and Johnson, 1999). The slope of a linear regression line fit through a plot of $1/\tau_o$ versus $[Mg^{2+}]_o$ (see Fig. 4*C*) was used to estimate $k_{+,app}$ based on the following equation: $1/\tau_{o,Mg} = 1/\tau_{o,control} + k_{+,app} \times [Mg^{2+}]_o$. $k_{-,app}$ was estimated as $1/\tau_b$.

Model fitting and simulations. Kinetic model fitting and predictions were made in SigmaPlot 2001 or SigmaPlot 8 (Systat Software, Point Richmond, CA). Data were weighted during fitting by the inverse of data value. Minimization of sum of squared errors (SSE) [this is equivalent to maximization of the coefficient of determination (R^2)] was used to achieve optimal fits. Fitting procedures and equations used are described in Results. Single-channel analysis of NR1/2D receptors is demanding because of their relatively low single-channel conductance and brief open time. In the presence of Mg_o^{2+}, dwell times were yet much briefer. The

Mg_o^{2+} inhibition at −45 mV. The voltage dependence of the effect of changing $[Na^+]_o$ on Mg_o^{2+} IC_{50} values measured from $[Mg^{2+}]_o$-inhibition curves is shown in Figure 2*C*. Changing $[Na^+]_o$ modestly affected Mg_o^{2+} IC_{50} of both receptors. The voltage dependence of the Na_o^+ effect differs between the two receptors, as will be further examined in Figure 3.

To illustrate the differential effects of permeant ions on Mg_o^{2+} inhibition of NR1/2A and NR1/2D receptors, we calculated the ratios of Mg_o^{2+} IC_{50} values in normal and low permeant ion concentrations (Fig. 3). A ratio of 1 indicates no effect of changing permeant ion concentration. The effect of changing $[Cs^+]_i$ on Mg_o^{2+} inhibition of both NR1/2A and NR1/2D receptors is large and strongly voltage dependent (Fig. 3*A*). At depolarized voltages, the effect of lowering $[Cs^+]_i$ became even greater for NR1/2D than NR1/2A receptors (at −15 mV, the Mg_o^{2+} IC_{50} ratio was 13.4 for NR1/2A but 32.9 for NR1/2D receptors). At hyperpolarized voltages, changing $[Cs^+]_i$ had a similar effect on NR1/2D and NR1/2A receptors. The effect of changing $[Na^+]_o$ on Mg_o^{2+} inhibition of both NR1/NR2A and NR1/NR2D receptors was small (Fig. 3*B*) (note different *y*-axis scales in Fig. 3*A*,*B*), although a difference in the voltage dependence of the ratio is apparent. The effect of lowering $[Na^+]_o$ on NR1/2D receptors was significantly voltage dependent ($p < 0.001$; two-tailed Pearson correlation test), causing a reduction of Mg_o^{2+} IC_{50} at hyperpolarized voltages but an increasing of Mg_o^{2+} IC_{50} at more depolarized voltages. The effect of changing $[Na^+]_o$ on NR1/2A receptors, in contrast, was not correlated with voltage ($p = 0.068$).

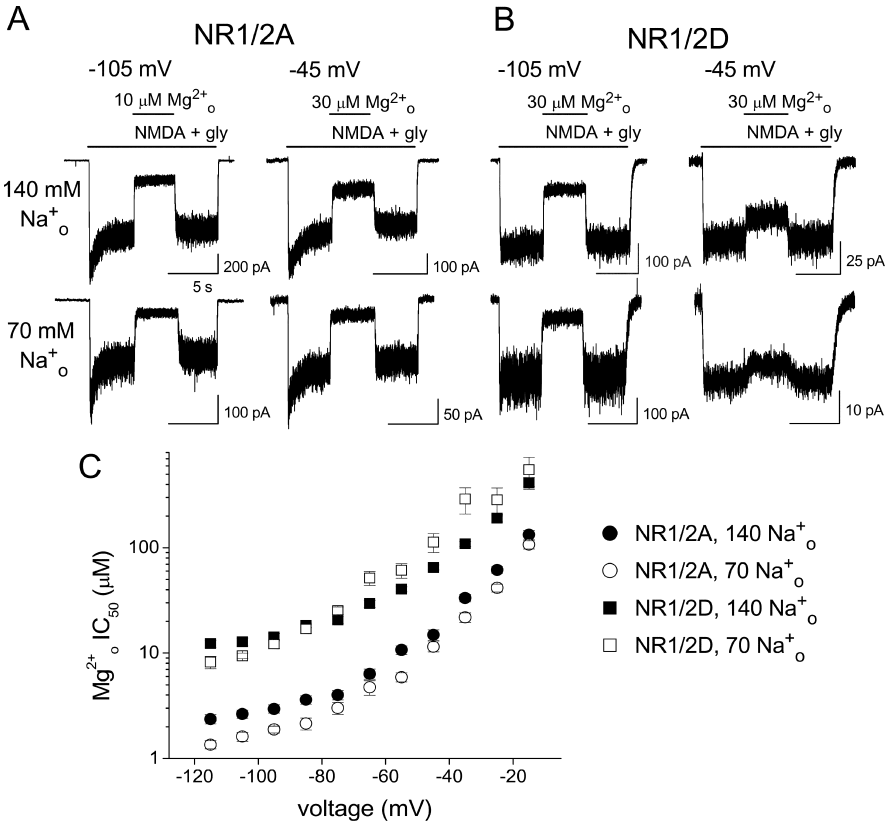

Figure 2. Effect of Na_o^+ on Mg_o^{2+} inhibition of NMDA receptor whole-cell currents. ***A***, ***B***, Examples of inhibition by Mg_o^{2+} of NR1/2A (***A***) and NR1/2D (***B***) receptor currents in 140 Na_o^+/8 Cs_i^+ (top traces) and 70 Na_o^+/8 Cs_i^+ (bottom traces) solutions at the indicated voltages. The bars above the current traces indicate the time of drug application. ***C***, Mg_o^{2+} IC_{50} values estimated from concentration–inhibition curves in 8 mM Cs_i^+ are plotted from −115 to −15 mV; subunit combination and $[Na^+]_o$ as indicated. Data collected in 140 Na_o^+/8 Cs_i^+ are replotted from Figure 1*D*. Error bars indicate SE.

The results presented so far suggest that permeant ions exert powerful effects on Mg_o^{2+} inhibition in NR1/2D as well as NR1/2A receptors. There are, however, intriguing differences between the two receptor subtypes. To investigate the mechanistic bases of these differences, we used single-channel analysis, which allowed us to examine the effect of changing permeant ion concentrations on Mg_o^{2+} blocking and unblocking steps separately.

Effect of changing $[Cs^+]_i$ and $[Na^+]_o$ on Mg_o^{2+} blocking and unblocking kinetics

Permeant ions powerfully affect Mg_o^{2+} block of NR1/2A receptors (Zhu and Auerbach, 2001a,b) and of NMDA receptors expressed in cultured cortical neurons (referred to here as cortical neurons) (Antonov and Johnson, 1999; Qian et al., 2002), which are composed of NR1, NR2A, and NR2B subunits (Monyer et al., 1994; Zhong et al., 1994; Kirson and Yaari, 1996; Antonov and Johnson, 1999; Qian et al., 2005). The similarity of the channels of cortical receptors and recombinant NR1/2A receptors is supported by their similar Mg_o^{2+} IC_{50} values in 140 Na_o^+/125 Cs_i^+ solution (Qian et al., 2005) and in solutions with lowered permeant ion concentrations (data not shown). Here, we report on the effects of changing $[Cs^+]_i$ and $[Na^+]_o$ on the Mg_o^{2+} $k_{+,app}$ and $k_{-,app}$ of recombinant NR1/2D receptors. In single-channel experiments,

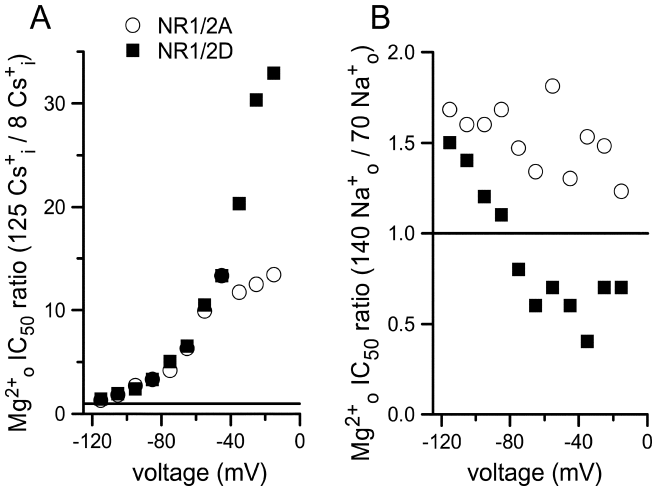

Figure 3. Differential effects of permeant ions on Mg_o^{2+} inhibition of NR1/2A and NR1/2D receptor whole-cell currents. ***A***, Ratio of Mg_o^{2+} IC_{50} measured in the 140 Na_o^+/125 Cs_i^+ and the 140 Na_o^+/8 Cs_i^+ solutions is plotted as a function of voltage for the indicated receptors. Changing $[Cs^+]_i$ has powerful voltage-dependent effects on both receptors; the effect is stronger on NR1/2D receptors at depolarized voltages. ***B***, Ratio of Mg_o^{2+} IC_{50} measured in the 140 Na_o^+/8 Cs_i^+ and the 70 Na_o^+/8 Cs_i^+ solutions plotted as a function of voltage for receptors as indicated in ***A***. Changing $[Na^+]_o$ has weak effects on Mg_o^{2+} IC_{50} that are voltage independent for NR1/2A receptors and voltage dependent for NR1/2D receptors. The horizontal lines show ratio values of 1 that would be expected if $[Cs^+]_i$ (***A***) or $[Na^+]_o$ (***B***) had no effect on Mg_o^{2+} IC_{50}.

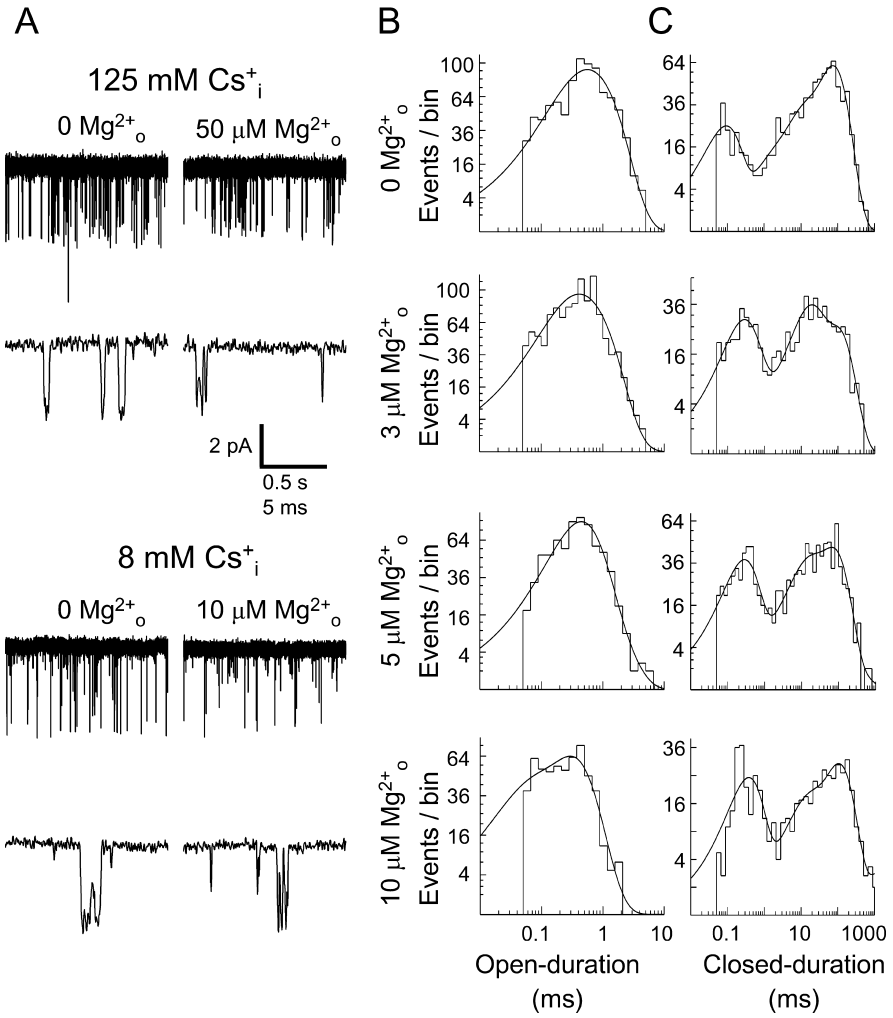

Figure 4. Effects of $[Cs^+]_i$ and $[Mg^{2+}]_o$ on single-channel openings of NR1/2D receptors. All data for this figure were collected at −85 mV. ***A***, Examples of Mg^{2+}_o-induced NR1/2D receptor single-channel "flicker." Traces in 0 Mg^{2+}_o (left) and in the indicated $[Mg^{2+}]_o$ (right) are shown in 140 Na^+_o/125 Cs^+_i (top) and in 140 Na^+_o/8 Cs^+_i (bottom). Two traces are shown for each condition at different time scales. Including Mg^{2+}_o caused channel flicker at lower $[Mg^{2+}]_o$ in 8 mM $[Cs^+]_i$ than in 125 mM $[Cs^+]_i$. ***B***, Open-duration histograms in 140 Na^+_o/8 Cs^+_i from the patch used for ***A*** in the indicated $[Mg^{2+}]_o$ values. The $[Mg^{2+}]_o$, and value of the time constant (and relative amplitude) of the largest component (τ_o), are as follows: 0 Mg^{2+}_o, 0.759 ms (76.4%); 3 μM Mg^{2+}_o, 0.603 ms (67.1%); 5 μM Mg^{2+}_o, 0.408 ms (77.1%); 10 μM Mg^{2+}_o, 0.301 ms (76.4%). The apparent blocking rate constant for Mg^{2+}_o ($k_{+,app}$) was estimated to be 179 $\mu M^{-1} s^{-1}$ for this patch. ***C***, Closed-duration histograms in 140 Na^+_o/8 Cs^+_i from the patch used for ***A*** in the indicated $[Mg^{2+}]_o$ values. The $[Mg^{2+}]_o$, and value of the time constant (and relative amplitude) of the component attributable to Mg^{2+}_o block (τ_b), are as follows: 3 μM Mg^{2+}_o, 0.375 ms (20.6%); 5 μM Mg^{2+}_o, 0.266 ms (34.5%); 10 μM Mg^{2+}_o, 0.355 ms (30.9%). The apparent unblocking rate for Mg^{2+}_o ($k_{-,app}$) was estimated to be 3081 s^{-1} for this patch.

we used three sets of ionic solutions: 140 Na^+_o/125 Cs^+_i, 140 Na^+_o/8 Cs^+_i, and 70 Na^+_o/25 Cs^+_i. These experimental conditions facilitated comparisons with previous cortical receptor single-channel recordings (Antonov and Johnson, 1999) and allowed exploration of a wide range of ionic conditions while limiting single-channel data collection, which is especially demanding with NR1/2D receptors. Use of these ionic conditions permitted direct determination of the effect of $[Cs^+]_i$ on the kinetics of Mg^{2+}_o block, but required model application (below) for quantification of the effects of $[Na^+]_o$.

Examples of single-channel NR1/2D receptor-mediated currents recorded in the absence and presence of Mg^{2+}_o, and in normal and low $[Cs^+]_i$s, are shown in Figure 4*A*. In normal $[Cs^+]_i$ (top), addition of 50 μM Mg^{2+}_o greatly increased channel "flicker," which reflects rapid transitions between the open and blocked states caused by Mg^{2+}_o channel block (Qian et al., 2005). In a low $[Cs^+]_i$ (bottom), this effect was achieved at a much lower $[Mg^{2+}]_o$, suggesting that $[Cs^+]_i$ influences Mg^{2+}_o block. The decrease in open duration associated with channel block, which was used to calculate $k_{+,app}$, is reflected in the open-duration histograms shown in Figure 4*B*. In the closed-duration histograms shown in Figure 4*C*, the closed-duration component that represents Mg^{2+}_o blocking events was used to calculate $k_{-,app}$.

The effects of changing permeant ion concentrations on the voltage dependence of Mg^{2+}_o block, unblock, and IC_{50} are shown in Figure 5. Lowering $[Cs^+]_i$ from 125 mM (black) to 8 mM (green) greatly increased Mg^{2+}_o $k_{+,app}$ (Fig. 5*A*). This effect was most prominent at depolarized voltages: at −105 mV, lowering $[Cs^+]_i$ increased $k_{+,app}$ 1.6-fold, whereas at −45 mV lowering $[Cs^+]_i$ increased $k_{+,app}$ 10-fold. Data in 70 Na^+_o/25 Cs^+_i (Fig. 5*A*, red) suggest that lowering $[Na^+]_o$ may increase $k_{+,app}$; if Na^+_o had no effect on $k_{+,app}$, these data would be intermediate between the data in 140 Na^+_o/125 Cs^+_i (black) and 140 Na^+_o/8 Cs^+_i (green). Lowering $[Cs^+]_i$ from 125 to 8 mM decreased $k_{-,app}$ in a voltage-dependent manner (Fig. 5*B*): at −45 mV, lowering $[Cs^+]_i$ decreased $k_{-,app}$ 1.5-fold ($p < 0.05$), whereas at −105 mV, lowering $[Cs^+]_i$ decreased $k_{-,app}$ 1.2-fold (not significant). Data in 70 Na^+_o/25 Cs^+_i (Fig. 5*B*, red) suggest that lowering $[Na^+]_o$ had only a weak effect on $k_{-,app}$. Also shown in Figure 5 (lines) are the results of modeling the effects of permeant ions on the Mg^{2+}_o $k_{+,app}$ (Fig. 5*A*), $k_{-,app}$ (Fig. 5*B*), and IC_{50} from whole-cell experiments (Fig. 5*C*).

Model of interaction of permeant ions and Mg^{2+}_o with NR1/2D receptors

To further interpret our whole-cell and single-channel data and better understand the mechanisms by which permeant ions and Mg^{2+}_o interact with NR1/2D receptors, we developed a quantitative model (the NR1/2D model) (see Fig. 7). We based the NR1/2D model on models previously used to describe the interaction of permeant ions and Mg^{2+}_o with cortical NMDA receptors (Antonov and Johnson, 1999; Qian et al., 2002) and NR1/2A receptors (Zhu and Auerbach, 2001a,b). We will focus on our previous work with cortical NMDA receptors because these data were collected under similar conditions. The effects of permeant ions on Mg^{2+}_o $k_{+,app}$ in the cortical NMDA receptor model are mediated by external permeant ion binding sites. Our data suggest that the effects of permeant ions on the Mg^{2+}_o $k_{+,app}$ of NR1/2D and cortical receptors are quite similar. Under the same conditions (ion concentrations and voltage), the Mg^{2+}_o $k_{+,app}$ values presented here were generally slightly lower for NR1/2D than cortical NMDA receptors (compare Fig. 5*A* with Antonov and Johnson, 1999, their Fig. 2*A*), but the differences were not statistically significant. Furthermore, the dramatic

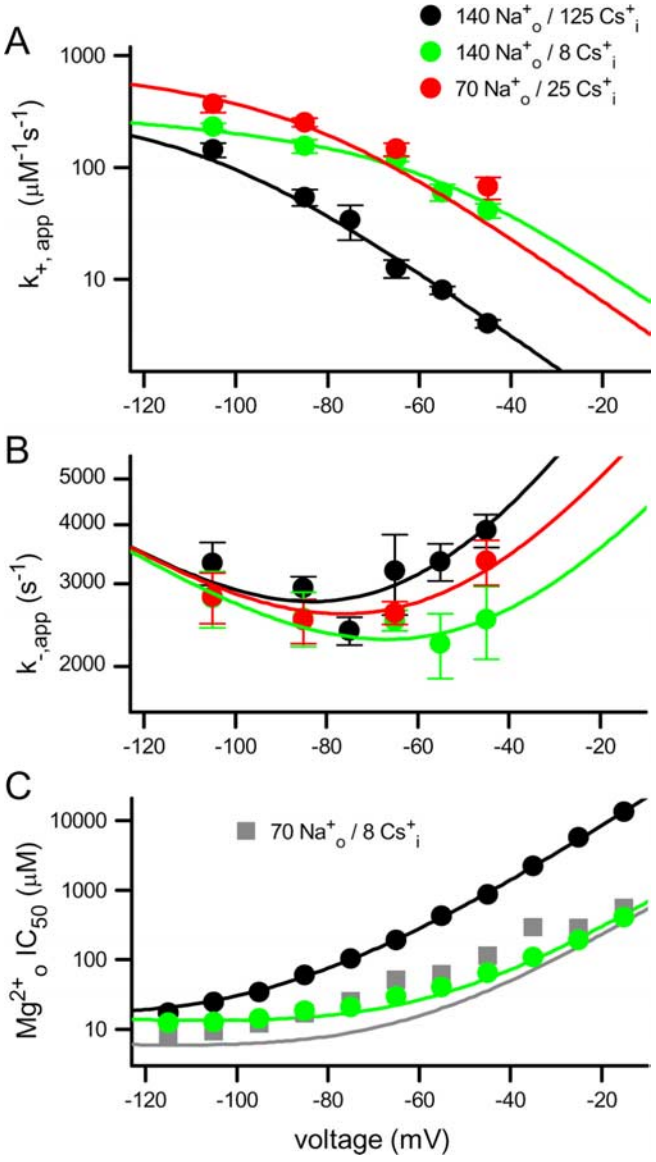

Figure 5. Effects of Cs_i^+ and Na_o^+ on Mg_o^{2+} block of NR1/2D receptors. ***A***, ***B***, Mg_o^{2+} $k_{+,app}$ (***A***) and $k_{-,app}$ (***B***) measured from single-channel recordings in the indicated solutions are plotted (symbols) as a function of voltage. Error bars indicate SEM. ***C***, Mg_o^{2+} IC_{50} measured from whole-cell recordings in the indicated solutions (symbols; black and green have same meaning as in ***A*** and ***B***) are plotted as a function of voltage. Whole-cell data collected in 70 Na_o^+/8 Cs_i^+ were not used in fitting (see Results). Data recorded in 140 Na_o^+/125 Cs_i^+ were replotted from Qian et al. (2005). The lines show NR1/2D model predictions using parameter values shown in Table 1 of $k_{+,app}$ (***A***), $k_{-,app}$ (***B***), and $K_D = k_{-,app}/k_{+,app}$ (***C***); the line colors have same meanings as symbol colors.

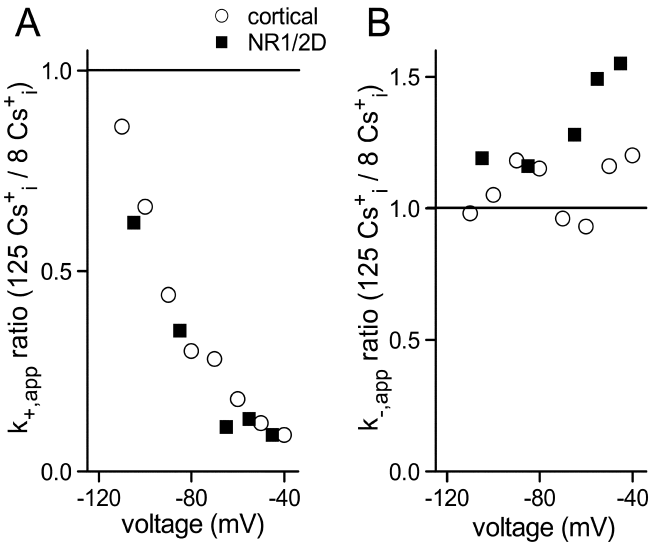

Figure 6. Effects of $[Cs^+]_i$ on Mg_o^{2+} $k_{+,app}$ and $k_{-,app}$ compared in cortical NMDA and NR1/2D receptors. ***A***, ***B***, Ratio of $k_{+,app}$ (***A***) and $k_{-,app}$ (***B***) measured in the 140 Na_o^+/125 Cs_i^+ and the 140 Na_o^+/8 Cs_i^+ solutions are plotted as a function of voltage for the indicated receptors. Cortical NMDA receptor data are from Antonov and Johnson (1999). The horizontal lines show ratio values of 1 that would be expected if $[Cs^+]_i$ had no effect on rates.

and strongly voltage-dependent effect of $[Cs^+]_i$ on $k_{+,app}$ is similar in NR1/2D receptors (Fig. 5*A*) and cortical NMDA receptors (Antonov and Johnson, 1999) (Fig. 6*A*). Based on these similarities, the NR1/2D model incorporates external permeant ion sites, as were found on cortical (Antonov and Johnson, 1999) and NR1/2A (Zhu and Auerbach, 2001a,b) receptors. Cs_i^+ can bind to one of the external sites and prevent Mg_o^{2+} from entering the channel (Na_o^+ can bind to either) (see below). The voltage dependence of the effect of changing $[Cs^+]_i$ originates from the voltage dependence of internal permeant ion access to the external site.

In contrast to $k_{+,app}$, the Mg_o^{2+} $k_{-,app}$ values of NR1/2D receptors and cortical NMDA receptors differ quantitatively and qualitatively. The Mg_o^{2+} $k_{-,app}$ is higher for NR1/2D receptors than cortical receptors at all voltages in physiological ion concentrations (Qian et al., 2005). Similarly, the Mg_o^{2+} $k_{-,app}$ is significantly higher for NR1/2D receptors than cortical receptors in 140 Na_o^+/8 Cs_i^+ at hyperpolarized potentials ($k_{-,app}$ values are significantly different at all voltages negative of −60 mV) (compare Fig. 5*B* with Antonov and Johnson, 1999, their Fig. 3*C*). Decreasing $[Cs^+]_i$, which had no effect on Mg_o^{2+} $k_{-,app}$ of cortical NMDA receptors at any voltage (Antonov and Johnson, 1999) (but see Zhu and Auerbach, 2001b), significantly reduced the Mg_o^{2+} $k_{-,app}$ of NR1/2D receptors at −45 mV (Figs. 5*B*, 6*B*). In whole-cell recordings (Fig. 3*A*), the effects of changing $[Cs^+]_i$ on the IC_{50} of NR1/2A and NR1/2D receptors diverged strongly at voltages depolarized of −50 mV. We hypothesized that the dependence of the NR1/2D receptor $k_{-,app}$ on $[Cs^+]_i$ (Figs. 5*B*, 6*B*), and the exaggerated dependence of the NR1/2D receptor IC_{50} on $[Cs^+]_i$ (Fig. 3*A*), are mediated by Cs^+ occupation of an internal permeant ion site. An internal permeant ion binding site has been observed on cortical receptors (Antonov et al., 1998) and NR1/2A receptors (Zhu and Auerbach, 2001b). However, an internal permeant ion site was not incorporated into our cortical NMDA receptor model because we observed no effect of $[Cs^+]_i$ on Mg_o^{2+} block in cortical receptors (Antonov and Johnson, 1999).

To test this hypothesis, we determined whether the effect of $[Cs^+]_i$ on $k_{-,app}$ could be reproduced by an NR1/2D model with an internal permeant ion site that can affect Mg_o^{2+} unblocking rate. In the NR1/2D model, Cs_i^+ occupation of the internal site while Mg_o^{2+} blocks the channel prevents Mg_o^{2+} permeation, and can accelerate unbinding of Mg_o^{2+} to the external solution, presumably through electrostatic repulsion. The voltage dependence of the effect of $[Cs^+]_i$ on $k_{-,app}$ was explained by permitting Cs_i^+ binding to be voltage dependent. Because changing $[Cs^+]_i$ had similar effects on the $k_{+,app}$ of cortical and NR1/2D receptors even at depolarized voltages (Fig. 6*A*), occupation of the internal site in the NR1/2D model does not affect the Mg_o^{2+} $k_{+,app}$. Binding of Cs_i^+ to the internal site when Mg_o^{2+} is not occupying the channel therefore is not shown in Figure 7 nor incorporated into the modeling equations below.

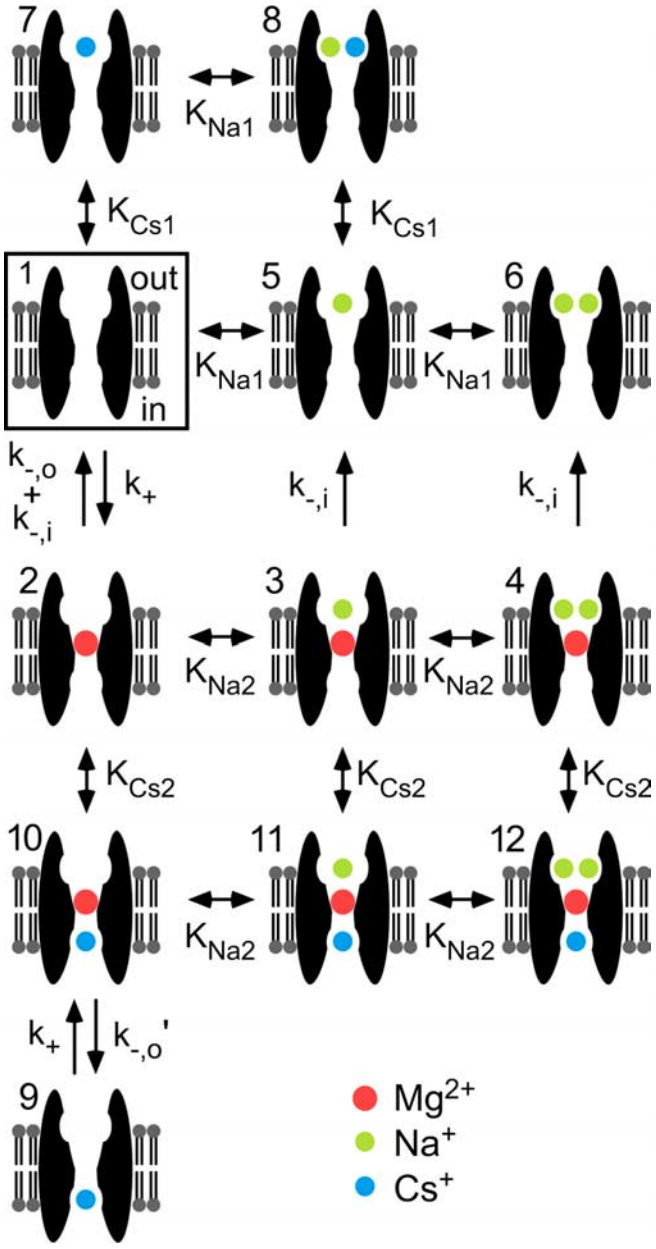

Figure 7. NR1/2D model of Mg_o^{2+} block. The central states of the model are 1 (boxed) and 2; transitions between states 1 and 2 represent Mg_o^{2+} unblock and block of the channel with no permeant ion bound. In states 1–8, the intracellular Cs_i^+ site is unoccupied; in states 3 and 4, Mg_o^{2+} cannot unblock to the extracellular solution because of the lock-in effect of Na_o^+; in states 5–8, Mg_o^{2+} cannot enter the channel because the external permeant ion sites are partly or fully occupied. States 9–12 correspond to states 1–4, respectively, except with a Cs_i^+ bound to the intracellular site. The single arrows represent modeled rates of transitions allowed in only one direction; the pairs of arrows represent transitions for which rates in each direction were modeled independently; the double-headed arrows represent transitions assumed to take place so rapidly that only dissociation constants were modeled. For each state, the upper side of the membrane faces the external solution and the lower side faces the internal solution.

As described previously, our data did not allow us to measure directly the effects of changing $[Na^+]_o$ on Mg_o^{2+} $k_{+,app}$ and $k_{-,app}$ in NR1/2D receptors. However, our results suggest that the effect of $[Na^+]_o$ on $k_{+,app}$ of NR1/2D and cortical receptors are similar, whereas the effect of $[Na^+]_o$ on $k_{-,app}$ of NR1/2D receptors appears weaker. To explain the effects of $[Na^+]_o$ on $k_{+,app}$, the characteristics of the external permeant ion binding sites on cortical receptors (Antonov and Johnson, 1999) were incorporated into the NR1/2D model: one or both sites can be occupied by Na^+ in a voltage-independent matter and prevent Mg_o^{2+} from entering the channel.

In cortical NMDA receptors, increasing $[Na^+]_o$ decreased $k_{-,app}$. This interaction was modeled by permitting Na_o^+ to bind to the external sites while Mg_o^{2+} blocked the channel, preventing Mg_o^{2+} unblock to the external solution by a "lock-in" effect (Antonov and Johnson, 1999). The apparently weaker effect of $[Na^+]_o$ on $k_{-,app}$ of NR1/2D receptors raises the question, can Na_o^+ bind while Mg_o^{2+} blocks the channel of this receptor? This question was addressed by incorporating into the NR1/2D model the ability for Na_o^+ to bind to the external sites and lock in a Mg_o^{2+} blocking the channel. However, in contrast to the previous model of cortical receptors (Antonov and Johnson, 1999), Na_o^+ affinity while Mg_o^{2+} blocks the channel can vary independently of the Na_o^+ affinity when the channel is unblocked.

The principal features of the NR1/2D model (Fig. 7) are as follows: (1) There are two external and one internal permeant ion binding sites. Cs_i^+ can occupy the internal site and one of the external sites; Na_o^+ can occupy either external site. Permeant ion binding to one site does not affect the affinity of ions for other site(s). Na_o^+ can bind to the external sites even when Mg_o^{2+} is bound in the channel, but with lower affinity. (2) Mg_o^{2+} can enter and block the channel only when the external sites are empty. (3) Mg_o^{2+} can unblock to the external solution only when both external sites are unoccupied by Na_o^+. Mg_o^{2+} also can unblock by permeating the channel. When the internal site is occupied by Cs_i^+, Mg_o^{2+} permeation is prevented and the rate Mg_o^{2+} unblock to the external solution is increased.

Model 1 is qualitatively distinct from the model previously developed for cortical NMDA receptors (Antonov and Johnson, 1999) in that model 1 incorporates an internal Cs_i^+ binding site.

Equations and fitting procedures

The equations derived to describe the NR1/2D model (Fig. 7) for $k_{+,app}$ (Eq. 2), $k_{-,app}$ (Eq. 3), and IC_{50} (Eq. 4) are as follows:

$$k_{+,app} = k_+ \times (1 + [Na^+]_o/K_{Na1})^{-1} \times (1 + [Na^+]_o/K_{Na1} + [Cs^+]_i/K_{Cs1})^{-1} \quad (2)$$

$$k_+ = k_+(0) \times \exp(V_m/V_1)$$

$$K_{Cs1} = K_{Cs1}(0) \times \exp(V_m/V_{Cs1})$$

$$k_{-,app} = k_{-,o} \times (1 + [Cs^+]_i/K_{Cs2})^{-1} \times (1 + [Na^+]_o/K_{Na2})^{-2} + k_{-,o}'(1 + K_{Cs2}/[Cs^+]_i)^{-1} \times (1 + [Na^+]_o/K_{Na2})^{-2} + k_{-,i} \times (1 + [Cs^+]_i/K_{Cs2})^{-1} \quad (3)$$

$$k_{-,o} = k_{-,o}(0) \times \exp(V_m/V_2)$$

$$k_{-,o}' = k_{-,o}(0)' \times \exp(V_m/V_2)$$

$$k_{-,i} = k_{-,i}(0) \times \exp(V_m/V_3)$$

$$K_{Cs2} = K_{Cs2}(0) \times \exp(V_m/V_{Cs2})$$

$$IC_{50} = k_{-,app}/k_{+,app}. \quad (4)$$

The meanings of the parameters are as follows [all of the 13 independent parameters that appear in the equations above (shown in bold) were allowed to vary during fitting]: $\boldsymbol{K_{Na1}}$, Na_o^+ equilibrium dissociation constant to the external site(s) with no Mg_o^{2+} bound; $\boldsymbol{K_{Na2}}$, Na_o^+ equilibrium dissociation constant to the external site(s) with Mg_o^{2+} bound; K_{Cs1}, Cs_i^+ pseudo-equilibrium dissociation constant for the external site; $\boldsymbol{K_{Cs1}(0)}$, K_{Cs1} at 0 mV;

$\boldsymbol{V_{Cs1}}$, voltage dependence of K_{Cs1} (mV for an *e*-fold change); K_{Cs2}, Cs_i^+ pseudo-equilibrium dissociation constant for the internal site with Mg_o^{2+} bound; $\boldsymbol{K_{Cs2}(0)}$, K_{Cs2} at 0 mV; $\boldsymbol{V_{Cs2}}$, voltage dependence of K_{Cs2}; $k_{+,app}$, apparent Mg_o^{2+} blocking rate constant; k_+, true (in the absence of permeant ions) Mg_o^{2+} blocking rate constant; $\boldsymbol{k_+(0)}$, k_+ at 0 mV; $\boldsymbol{V_1}$, voltage dependence of k_+; $k_{-,app}$, apparent Mg_o^{2+} unblocking rate; $k_{-,o}$, Mg_o^{2+} unblocking rate to the outside without Cs_i^+ bound at the internal site; $\boldsymbol{k_{-,o}(0)}$, $k_{-,o}$ at 0 mV; $\boldsymbol{V_2}$, voltage dependence of $k_{-,o}$ and $k_{-,o}'$; $k_{-,o}'$, Mg_o^{2+} unblocking rate to the outside with Cs_i^+ bound at the internal site; $\boldsymbol{k_{-,o}(0)'}$, $k_{-,o}'$ at 0 mV; $k_{-,i}$, true rate of Mg_o^{2+} permeation; $\boldsymbol{k_{-,i}(0)}$, $k_{-,i}$ at 0 mV; $\boldsymbol{V_3}$, voltage dependence of $k_{-,i}$; and IC_{50}, $[Mg^{2+}]_o$ at which whole-cell NMDA responses are inhibited by 50%.

Table 1. Comparison of NR1/2D and cortical NMDA receptor model parameter values

Description	Parameter	NR1/2D model	Cortical NMDA receptor model
Mg_o^{2+} blocking rate	$k_+(0)$ ($\mu M^{-1} s^{-1}$)	1170	1100
	V_1 (mV)	−138	−55.0
	δ_1	0.0922	0.231
Mg_o^{2+} outward unblocking rate	$k_{-,o}(0)$ (s^{-1})	7,420	110,000
	$k_{-,o}(0)'$ (s^{-1})	>34,600[a]	
	V_2 (mV)	38.7	52.7
	δ_2	0.329	0.241
Mg_o^{2+} inward unblocking rate	$k_{-,i}(0)$ (s^{-1})	556	61.8
	V_3 (mV)	−68.7	−50.0
	δ_3	0.185	0.254
Na^+ dissociation constants, external site	K_{Na1} (mM)	59.7	34.4
	K_{Na2} (mM)	452	34.4[b]
Cs^+ dissociation constant, external site	$K_{Cs1}(0)$ (mM)	0.0793	0.270
	V_{Cs1} (mV)	−16.9	−21.0
Cs^+ dissociation constant, internal site	$K_{Cs2}(0)$ (mM)	>116[a]	
	V_{Cs2} (mV)	−94	
	δ_4	0.271	

The voltage dependence of rate and dissociation constants was used to estimate electrical depths (δ) of barriers and binding sites (Woodhull, 1973).

[a]See Results for description of how minimum values were estimated. Values used for NR1/2D model predictions were as follows: 15.5 M [$K_{Cs2}(0)$] and 1.71×10^6 s^{-1} [$k_{-,o}(0)'$].

[b]K_{Na2} was set equal to K_{Na1} in the model of cortical NMDA receptors (Antonov and Johnson, 1999).

To constrain the model as well as possible during fitting, the following eight data sets (Fig. 5) were simultaneous fit: (1) $k_{+,app}$ in 140 Na_o^+/125 Cs_i^+; (2) $k_{+,app}$ in 140 Na_o^+/8 Cs_i^+; (3) $k_{+,app}$ in 70 Na_o^+/25 Cs_i^+; (4) $k_{-,app}$ in 140 Na_o^+/125 Cs_i^+; (5) $k_{-,app}$ in 140 Na_o^+/8 Cs_i^+; (6) $k_{-,app}$ in 70 Na_o^+/25 Cs_i^+; (7) whole-cell measured IC_{50} values in 140 Na_o^+/125 Cs_i^+; (8) IC_{50} value in 140 Na_o^+/8 Cs_i^+. Data sets 1–6 were from single-channel experiments, and 7 and 8 were from whole-cell experiments. Simultaneous fitting of single-channel measurements of Mg_o^{2+} block kinetics and whole-cell measurement of Mg_o^{2+} IC_{50} was valid because of the excellent agreement between IC_{50} and K_D ($=k_{-,app}/k_{+,app}$) values (for the 140 Na_o^+/125 Cs_i^+ solution, see Qian et al., 2005; for 140 Na_o^+/8 Cs_i^+ solution, data not shown). Although this implies that data sets 7 and 8 are redundant with data sets 1, 2, 4, and 5, simultaneous fitting of whole-cell along with single-channel data provided several advantages: whole-cell experiments were performed over a wider voltage range; IC_{50} was measured with much greater precision than $k_{-,app}$ and $k_{+,app}$ because IC_{50} measurements were based on more data points measured with lower noise; the model was fit to data from independent experiments with different recording techniques.

Whole-cell data collected in 70 Na_o^+/8 Cs_i^+ were not used for fitting because single-channel recordings in these ionic conditions were not made, preventing us from determining whether IC_{50} and $k_{-,app}/k_{+,app}$ values agree. Thus, the Mg_o^{2+} IC_{50} values in 70 Na_o^+/8 Cs_i^+ were not fit, but were predicted with the NR1/2D model (Fig. 5*C*). The agreement between lines and data are poorer for the Mg_o^{2+} IC_{50} values in 70 Na_o^+/8 Cs_i^+ than for other data. This remained true, although to a lesser extent, even when the Mg_o^{2+} IC_{50} values in 70 Na_o^+/8 Cs_i^+ were included during the fitting procedure. The reason for this discrepancy is unclear. It is worth noting that the model of cortical NMDA receptors (Qian et al., 2002) also fails to provide very accurate predictions for Mg_o^{2+} IC_{50} data collected in 70 Na_o^+/8 Cs_i^+. It is possible that with low permeant ion concentrations, channel gating or receptor conformation is altered so that the parameter values determined at higher ion concentrations no longer are accurate.

Before choosing the NR1/2D model described above, many alternative models were tested and discarded. Simpler models were discarded because they provided inferior fits based on appearance and SSE (for example, a model with no internal permeant ion binding site); more complex models were discarded because they increased the number of adjustable parameters without a corresponding improvement in quality of fit (for example, a model in which binding of Cs^+ to the internal site can decrease the rate of Mg_o^{2+} block). Some model modifications had only small effects on the quality of fits, suggesting limitations to our ability to describe NR1/2D receptor channel properties based on the data presented here (see next section).

Fitting results

The results of simultaneous fitting of whole-cell and single-channel data are shown in Figure 5 (lines) and the parameter values that provided the best fit (lowest SSE) are listed in Table 1. The NR1/2D model provides satisfactory fits to both whole-cell and single-channel data (global $R^2 = 0.996$), indicating that the hypotheses used to develop model 1 are consistent with data.

The parameter values shown in Table 1 provide insight into similarities and differences between NR1/2D and cortical receptors. In the absence of permeant ions, the blocking rates of Mg_o^{2+} at 0 mV [$k_+(0)$] for NR1/2D and cortical receptors are remarkably close. Na_o^+ and Cs_i^+ also exhibit similar affinities for the external permeant ion sites on NR1/2D and cortical receptors. These observations suggest that there is little difference between the external entryways to the channels of NR1/2D and cortical receptors. Rates of Mg_o^{2+} efflux, on the other hand, differ dramatically in NR1/2D and cortical receptors: efflux to the external solution [$k_{-,o}(0)$] is >10-fold faster for cortical receptors, whereas the permeation rate [$k_{-,i}(0)$] is nearly 10-fold faster in NR1/2D receptors. Evidence for an internal permeant ion binding site was observed only in NR1/2D receptors. These observations suggest that inner regions of the channel, including the Mg_o^{2+} binding site, the selectivity filter, and the intracellular channel entrance, differ most strongly in NR1/2D and cortical receptors.

Examples of the net effect of differences in Mg_o^{2+} binding and permeant ion binding to NR1/2D and cortical receptors in physiological permeant ion concentrations are shown in Table 2. Both model-based and, where possible, experimentally determined

Table 2. Mg_o^{2+} block properties of NR1/2D and cortical NMDA receptors at −55 mV

Parameter	NR1/2D receptors		Cortical NMDA receptors	
	Measured	Modeled	Measured	Modeled
IC_{50} (μM)	425		116	
$K_{D,app}$ (μM)	483	412	136	116
$k_{+,app}$ ($\mu M^{-1} s^{-1}$)	7.40	8.14	13.1	14.6
$k_{-,app}$ (s^{-1})	3575	3352	1788	1694
$k_{-,o,app}$ (s^{-1})		2119		1508
$k_{-,i,app}$ (s^{-1})		1233		186

All values are for the 140 Na^+/125 Cs^+ solution.

rates and dissociation constants that characterize Mg_o^{2+} block are shown. A voltage of −55 mV was used because it is within the voltage range used for measurements, eliminating extrapolation errors, and because physiologically significant Mg_o^{2+} unblock occurs near −55 mV. At this voltage, one or both of the external permeant ion sites of either receptor is occupied (meaning that Mg_o^{2+} cannot enter the channel) close to 99.5% of the time; the sites are occupied even more often as voltage is depolarized. Thus, the Mg_o^{2+} blocking rates are slowed ~200-fold by permeant ions at −55 mV, emphasizing the powerful control of the external permeant ion sites on block (see also Discussion and Fig. 8). The approximately fourfold difference in the Mg_o^{2+} IC_{50} of NR1/2D and cortical receptors at −55 mV results from differences both in Mg_o^{2+} blocking rate (almost twofold faster for cortical receptors) and Mg_o^{2+} unblocking rate (twofold faster for NR1/2D receptors). Consistent with the idea that the selectivity filters of NR1/2D and cortical receptors differ strongly, the most striking difference in Table 2 is in the rate of Mg_o^{2+} permeation (over six times faster for NR1/2D receptors).

Based on fits of modified models to our data, the values of three parameters [K_{Na2}, $K_{Cs2}(0)$, and $k_{-,o}(0)'$] could not be determined with useful accuracy by fitting of the NR1/2D model. Only modest increases in SSE (small decreases in goodness of fit) were achieved when fits were performed with K_{Na2} constrained to any of a wide range of values greater than K_{Na1}. Thus, the data suggest that Na_o^+ affinity for the external site decreases when Mg_o^{2+} blocks the channel, but we cannot accurately estimate the magnitude of the effect. The values of $K_{Cs2}(0)$ and $k_{-,o}(0)'$ that resulted from unconstrained model fitting (15.5 M and $1.71 \times 10^6\ s^{-1}$, respectively) would suggest that Cs_i^+ very rarely binds to the internal site, but when it binds, Mg_o^{2+} unblock is vastly accelerated. However, we found that fits of nearly equal quality resulted when both $K_{Cs2}(0)$ and $k_{-,o}(0)'$ were greatly decreased. The values shown in Table 1 are the minimum values that provided adequate fits (fits with SSE no more than twofold greater than the SSE of unconstrained fits) with all other parameters constrained to the values shown in Table 1. Thus, the actual values of $K_{Cs2}(0)$ and $k_{-,o}(0)'$ are likely to be larger than the values shown in Table 1.

Discussion

NR1/2D and NR1/2C receptors exhibit much weaker inhibition by Mg_o^{2+} than NR1/2A or NR1/2B receptors. To investigate the mechanistic basis of these differences, we developed a quantitative model of the interaction of Mg_o^{2+} and permeant ions with NR1/2D receptors. Here, we integrate current results with previous data predominantly from NR1/2D and cortical receptors.

Comparison of NR1/2D and cortical receptors

First, we will consider predicted differences in Mg_o^{2+} block in the absence of permeant ions. In Figure 8*A*, the energy profile of NR1/2D receptor channels (predicted with the NR1/2D model developed here) and cortical receptors [predicted with the model of Antonov and Johnson (1999)] in the absence of permeant ions are compared. The barrier height (*y*-axis) for entry into either channel is nearly identical. The electrical location of the Mg_o^{2+} binding site (location on *x*-axis of minima in the energy profiles) is slightly shallower in NR1/2D ($\delta = 0.42$) than in cortical ($\delta = 0.47$) receptors. This small difference may explain the decreased Na_o^+ affinity for the external site during Mg_o^{2+} block ($K_{Na2} > K_{Na1}$): a shallower blocking site may lead to repulsion of external permeant ions by Mg_o^{2+} during block. The energy well at which Mg_o^{2+} blocks is deeper in NR1/2D than in cortical receptors. This surprising result can be reconciled with the observation that Mg_o^{2+} IC_{50} is higher for NR1/2D receptors by considering the effects of permeant ions (below). The permeation barrier is much lower for NR1/2D than cortical receptors; as a result, Mg_o^{2+} permeates much faster through NR1/2D receptors.

We observed that external permeant ion sites, which have a powerful influence on Mg_o^{2+} inhibition of cortical receptors, also are present and exhibit similar properties on NR1/2D receptors. An internal permeant ion site, which we previously observed not to influence Mg_o^{2+} unblock from cortical receptors, did affect Mg_o^{2+} unblock from NR1/2D receptors. The enormous influence of permeant ions on Mg_o^{2+} block of both NR1/2D and cortical receptors is illustrated in Figure 8*B–D*. The extremely fast Mg_o^{2+} blocking rates (Fig. 8*B*, left) in the absence of permeant ions (dashed lines) are slowed dramatically by occupation of the permeant ion sites (solid lines). The voltage dependences of the Mg_o^{2+} blocking rate for NR1/2D and cortical receptors are greatly exaggerated by the external permeant ion sites because of the voltage dependence of Cs_i^+ binding (Antonov and Johnson, 1999). The weak voltage dependence of Mg_o^{2+} blocking rates in the absence of permeant ions (Fig. 8*B*, left, dashed lines) reflects the relatively shallow location of the barrier to Mg_o^{2+} entry into the channel (Fig. 8*A*).

Mg_o^{2+} unblocking rates of NR1/2D and cortical receptors (Fig. 8*B*, right) differ strongly. Permeant ions impact Mg_o^{2+} unblock from cortical receptors much more strongly because Na_o^+ can lock Mg_o^{2+} into the channel, an effect that is weak or absent in NR1/2D receptors. However, Cs_i^+ binding to the internal permeant ion site at positive potentials accelerates Mg_o^{2+} unbinding from NR1/2D receptors, a phenomenon we did not find in cortical receptors. The curvature of the Mg_o^{2+} unblocking rate plot is greater for NR1/2D than cortical receptor because of much faster permeation, which accelerates with hyperpolarization.

The influence of the permeant ion binding sites on NMDA receptor *I–V* curves is shown in Figure 8, *C* and *D*. It should not be surprising that permeant ion binding exerts strong control over channel block based on extensive precedent from the K^+ channel literature (Hille and Schwarz, 1978; Spassova and Lu, 1998; Guo et al., 2003). Nevertheless, the magnitude of the effect of the permeant ion sites on inhibition by Mg_o^{2+} is impressive. Without the permeant ion sites, Mg_o^{2+} channel block would prevent NR1/2D and cortical receptors from passing significant inward current at any physiological voltage (Fig. 8*C*,*D*, dotted lines). The decrease in Mg_o^{2+} inhibition caused by permeant ion sites can be appreciated by comparing the slopes of the *I–V* curves in the lower graphs of Figure 8, *C* and *D*, or by comparing Mg_o^{2+}

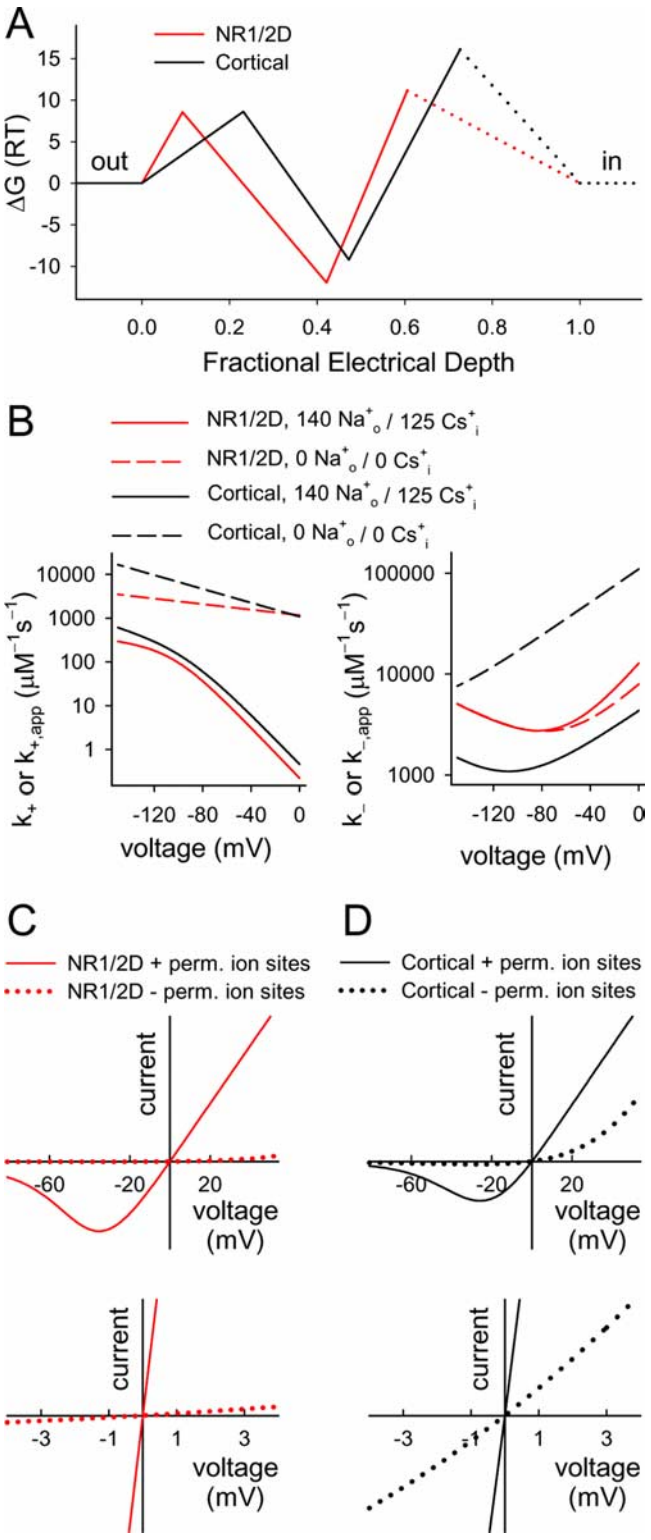

Figure 8. Comparison of NR1/2D and cortical receptor modeling results. ***A***, Schematic energy profiles for Mg_o^{2+} interaction with NR1/2D (red line) and cortical (black line) receptors. Rate theory was used to estimate barrier heights and well depths from the equation $\Delta G_i = -\ln(k_i/(6.11 \times 10^{12}\ s^{-1}))$, where ΔG_i is the plotted Gibbs free energy difference between two states (units of RT, where R is the gas constant and T is absolute temperature) and k_i is the rate constant for transitions between the states (Li-Smerin and Johnson, 1996; Hille, 2001). By convention, a $[Mg^{2+}]$ of 1 M is assigned the 0 energy state. Although fraught with inaccuracies (Nonner et al., 1999), rate theory estimates of energy profiles allow useful visual comparisons of kinetic data (Miller, 1999). Electrical depths (*x*-axis) are taken from Table 1. The dotted lines indicate regions in which the energy profile is unaddressed by the current data; the Mg^{2+} binding site on the internal side of cortical receptors (Johnson and Ascher, 1990), e.g., is not shown. ***B***, Model predictions of Mg_o^{2+} blocking (left) and un- blocking (right) rates are plotted for the indicated receptors and solutions. NR1/2D receptor predictions from the NR1/2D model; cortical receptor predictions from model of Antonov and Johnson (1999). k_- is sum of the unblocking rate to the outside and permeation rate. ***C***, ***D***, Predicted NMDA receptor *I–V* curves in the 140 Na_o^+/125 Cs_i^+ solution with 1 mM Mg_o^{2+}. *I–V* curve in 0 Mg was assumed to be linear with a reversal potential of 0 mV. The bottom graphs are blowups of the region near the origin of top graphs. The solid lines show predictions of the NR1/2D model (***C***; red) or the cortical receptor model from Antonov and Johnson (1999) (***D***; black), and the dotted lines show predictions of modified models that are identical except with no permeant ion binding sites.

IC_{50} values. At 0 mV, the predicted Mg_o^{2+} IC_{50} values without and with the permeant ion binding sites are as follows: NR1/2D receptors, 6.82 μM and 57.4 mM; cortical receptors, 100 μM and 9.8 mM. The much greater effect of the permeant ion sites on the Mg_o^{2+} IC_{50} of NR1/2D receptors results predominantly from three differences: (1) increased outward unbinding of Mg_o^{2+} from NR1/2D receptors when the internal permeant ion binding site is occupied; (2) decreased outward unbinding of Mg_o^{2+} from cortical receptors when external Na_o^+ locks Mg_o^{2+} in; (3) decreased rate of Mg_o^{2+} binding to NR1/2D receptors because of the higher affinity of Cs_i^+ for the external permeant ion site.

Although there is no internal permeant ion site in the cortical NMDA receptor model of Antonov and Johnson (1999), there is considerable evidence for such a site (Antonov et al., 1998; Zhu and Auerbach, 2001b). Furthermore, Mg_i^{2+} can bind to an internal site on cortical receptors (Johnson and Ascher, 1990; Li-Smerin and Johnson, 1996); the relationship between the internal permeant ion and Mg_i^{2+} sites is unknown. It is possible that the internal permeant ion site on cortical receptors has little effect on Mg_o^{2+} unblock because of lower permeant ion affinity than the site on NR1/2D receptors. Alternatively, the site on NR1/2D receptors may be deeper in the channel, closer to the Mg_o^{2+} blocking site. Finally, NR2 subunit-dependent differences in the K^+ versus Cs^+ selectivity of the internal site cannot be excluded; the internal site on NR1/2A receptors is selective for K^+ over Na^+ (Zhu and Auerbach, 2001a).

A slow component of Mg_o^{2+} unblock (Vargas-Caballero and Robinson, 2003) recently was reported to be NR2 subunit dependent: slow unblock is observed with NR1/2A and NR1/2B receptors, but not with NR1/2C and NR1/2D receptors (Clarke and Johnson, 2006). The greater ability of Na_o^+ to lock Mg_o^{2+} into its blocking site on cortical than NR1/2D receptors might appear to provide an explanation for slow Mg_o^{2+} unblock differences. However, both the NR1/2D and cortical models predict much faster Mg_o^{2+} unblock than the slow components observed with NR1/2A and NR1/2B receptors. Thus, the data presented here cannot explain the NR2 subunit dependence of slow Mg_o^{2+} unblock.

Implications for channel structure

We concluded that the external channel entrance as seen by Mg_o^{2+} and Na^+ is similar in NR1/2D and cortical receptors. The Mg_o^{2+} binding site differs moderately in the channels of the two receptors. The greatest differences appear toward the intracellular end of the channel, where Mg^{2+} permeates much more quickly through NR1/2D receptors, and internal permeant ions bind with much greater affinity.

Kuner and Schoepfer (1996) examined regions of NMDA receptors that underlie the subunit dependence of Mg_o^{2+} inhibition. They found that the M1, M2–M3 linker, and M4 regions all contribute to subunit-dependent differences, but that the M2 region does not. Our data do not disagree with these conclusions, be-

cause the M1, M2–M3 linker, and M4 regions all could influence, either directly or indirectly, the internal region of the channel.

Because the structure of the channel of NMDA receptors is mostly unknown, the relationship of the external and internal permeant ion sites to the rest of the channel can only be speculated. However, hypotheses can be proposed based on the evidence for at least a global structural similarity between glutamate receptor channels and inside-out K^+ channels (Chen et al., 1999; Panchenko et al., 2001; Kuner et al., 2003; Wollmuth and Sobolevsky, 2004). The internal "cavity" of K^+ channels is thought to hold a single ion, and to exhibit little ion selectivity (Doyle et al., 1998). A plausible location for the external permeant ion binding sites of NMDA receptors would be an analogous cavity that can hold two monovalent cations. Because Mg_o^{2+} would pass through the cavity en route to its blocking site, occupancy of the cavity by permeant ions may preclude Mg_o^{2+} access to its blocking site. Lock-in of Mg_o^{2+} during block by occupation of the same cavity by permeant ions is plausible, in analogy with lock-in of Ba^{2+} while blocking K^+ channels by internal monovalent cations (Neyton and Miller, 1988; Jiang and MacKinnon, 2000). The internal permeant ion site on NMDA receptors may resemble an external cavity on NaK channels, which are structurally related to K^+ channels (Shi et al., 2006).

Physiological implications

The permeant ion binding sites powerfully regulate the affinity and voltage dependence of Mg_o^{2+} block under physiological conditions. Without the permeant ion binding sites, Mg_o^{2+} block of NMDA receptors would almost fully inhibit current would flow (Fig. 8*C*,*D*); Mg_o^{2+} would have higher affinity for NR1/2D than cortical receptors; voltage dependence of block would be much weaker (Fig. 8*B*). Variations in permeant ion concentrations also may modulate Mg_o^{2+} inhibition under physiological or pathological conditions. Large local changes in ion concentrations are observed during normal synaptic transmission, and much greater changes occur in pathological states (Grisar, 1984; Lux et al., 1986; Kager et al., 2000; Rose and Konnerth, 2001). These changes in permeant ion concentrations would greatly affect Mg_o^{2+} inhibition. Based on the data presented here, the magnitude of the effect would be NR2 subunit dependent.

References

Aizenman E, Sinor JD, Brimecombe JC, Herin GA (2000) Alterations of *N*-methyl-D-aspartate receptor properties after chemical ischemia. J Pharmacol Exp Ther 295:572–577.

Antonov SM, Johnson JW (1999) Permeant ion regulation of *N*-methyl-D-aspartate receptor channel block by Mg^{2+}. Proc Natl Acad Sci USA 96:14571–14576.

Antonov SM, Gmiro VE, Johnson JW (1998) Binding sites for permeant ions in the channel of NMDA receptors and their effects on channel block. Nat Neurosci 1:451–461.

Bengzon J, Okabe S, Lindvall O, McKay RD (1999) Suppression of epileptogenesis by modification of *N*-methyl-D-aspartate receptor subunit composition. Eur J Neurosci 11:916–922.

Buller AL, Monaghan DT (1997) Pharmacological heterogeneity of NMDA receptors: characterization of NR1a/NR2D heteromers expressed in *Xenopus* oocytes. Eur J Pharmacol 320:87–94.

Chen GQ, Cui C, Mayer ML, Gouaux E (1999) Functional characterization of a potassium-selective prokaryotic glutamate receptor. Nature 402:817–821.

Chen L, Huang LY (1992) Protein kinase C reduces Mg^{2+} block of NMDA-receptor channels as a mechanism of modulation. Nature 356:521–523.

Clarke RJ, Johnson JW (2006) NMDA receptor NR2 subunit dependence of the slow component of magnesium unblock. J Neurosci 26:5825–5834.

Colquhoun D, Sigworth FJ (1995) Fitting and statistical analysis of single-channel records. In: Single-channel recording (Sakmann B, Neher E, eds), pp 483–587. New York: Plenum.

Cull-Candy SG, Leszkiewicz DN (2004) Role of distinct NMDA receptor subtypes at central synapses. Sci STKE 2004:re16.

Dingledine R, Borges K, Bowie D, Traynelis SF (1999) The glutamate receptor ion channels. Pharmacol Rev 51:7–61.

Doyle DA, Morais Cabral J, Pfuetzner RA, Kuo A, Gulbis JM, Cohen SL, Chait BT, MacKinnon R (1998) The structure of the potassium channel: molecular basis of K^+ conduction and selectivity. Science 280:69–77.

Furukawa Y, Okada M, Akaike N, Hayashi T, Nabekura J (2000) Reduction of voltage-dependent magnesium block of *N*-methyl-D-aspartate receptor-mediated current by in vivo axonal injury. Neuroscience 96:385–392.

Grisar T (1984) Glial and neuronal Na^+-K^+ pump in epilepsy. Ann Neurol 16:S128–S134.

Guo D, Ramu Y, Klem AM, Lu Z (2003) Mechanism of rectification in inward-rectifier K^+ channels. J Gen Physiol 121:261–276.

Guo H, Huang LY (2001) Alteration in the voltage dependence of NMDA receptor channels in rat dorsal horn neurones following peripheral inflammation. J Physiol (Lond) 537:115–123.

Hamill OP, Marty A, Neher E, Sakmann B, Sigworth FJ (1981) Improved patch-clamp techniques for high-resolution current recording from cells and cell-free membrane patches. Pflügers Arch 391:85–100.

Hille B (2001) Ion channels of excitable membranes, Ed 3. Sunderland, MA: Sinauer.

Hille B, Schwarz W (1978) Potassium channels as multi-ion single-file pores. J Gen Physiol 72:409–442.

Hori N, Carpenter DO (1994) Transient ischemia causes a reduction of Mg^{2+} blockade of NMDA receptors. Neurosci Lett 173:75–78.

Hrabetova S, Serrano P, Blace N, Tse HW, Skifter DA, Jane DE, Monaghan DT, Sacktor TC (2000) Distinct NMDA receptor subpopulations contribute to long-term potentiation and long-term depression induction. J Neurosci 20:RC81(1–6).

Jiang Y, MacKinnon R (2000) The barium site in a potassium channel by x-ray crystallography. J Gen Physiol 115:269–272.

Johnson JW, Ascher P (1990) Voltage-dependent block by intracellular Mg^{2+} of *N*-methyl-D-aspartate-activated channels. Biophys J 57:1085–1090.

Kager H, Wadman WJ, Somjen GG (2000) Simulated seizures and spreading depression in a neuron model incorporating interstitial space and ion concentrations. J Neurophysiol 84:495–512.

Kato N, Yoshimura H (1993) Reduced Mg^{2+} block of *N*-methyl-D-aspartate receptor-mediated synaptic potentials in developing visual cortex. Proc Natl Acad Sci USA 90:7114–7118.

Kirson ED, Yaari Y (1996) Synaptic NMDA receptors in developing mouse hippocampal neurones: functional properties and sensitivity to ifenprodil. J Physiol 497:437–455.

Kuner T, Schoepfer R (1996) Multiple structural elements determine subunit specificity of Mg^{2+} block in NMDA receptor channels. J Neurosci 16:3549–3558.

Kuner T, Wollmuth LP, Karlin A, Seeburg PH, Sakmann B (1996) Structure of the NMDA receptor channel M2 segment inferred from the accessibility of substituted cysteines. Neuron 17:343–352.

Kuner T, Seeburg PH, Guy HR (2003) A common architecture for K^+ channels and ionotropic glutamate receptors? Trends Neurosci 26:27–32.

Lisman JE, McIntyre CC (2001) Synaptic plasticity: a molecular memory switch. Curr Biol 11:R788–R791.

Li-Smerin Y, Johnson JW (1996) Kinetics of the block by intracellular Mg^{2+} of the NMDA-activated channel in cultured rat neurons. J Physiol 491:121–135.

Lux HD, Heinemann U, Dietzel I (1986) Ionic changes and alterations in the size of the extracellular space during epileptic activity. Adv Neurol 44:619–639.

Marty A, Neher E (1995) Tight-seal whole-cell recording. In: Single-channel recording (Sakmann B, Neher E, eds), pp 31–52. New York: Plenum.

Miller C (1999) Ionic hopping defended. J Gen Physiol 113:783–787.

Miyamoto Y, Yamada K, Noda Y, Mori H, Mishina M, Nabeshima T (2002) Lower sensitivity to stress and altered monoaminergic neuronal function in mice lacking the NMDA receptor ε4 subunit. J Neurosci 22:2335–2342.

Momiyama A, Feldmeyer D, Cull-Candy SG (1996) Identification of a native low-conductance NMDA channel with reduced sensitivity to Mg^{2+} in rat central neurones. J Physiol 494:479–492.

Monyer H, Burnashev N, Laurie DJ, Sakmann B, Seeburg PH (1994) Devel-

opmental and regional expression in the rat brain and functional properties of four NMDA receptors. Neuron 12:529–540.

Nakazawa K, Quirk MC, Chitwood RA, Watanabe M, Yeckel MF, Sun LD, Kato A, Carr CA, Johnston D, Wilson MA, Tonegawa S (2002) Requirement for hippocampal CA3 NMDA receptors in associative memory recall. Science 297:211–218.

Neher E, Steinbach JH (1978) Local anaesthetics transiently block currents through single acetylcholine-receptor channels. J Physiol (Lond) 277:153–176.

Neyton J, Miller C (1988) Potassium blocks barium permeation through a calcium-activated potassium channel. J Gen Physiol 92:549–567.

Nonner W, Chen DP, Eisenberg B (1999) Progress and prospects in permeation. J Gen Physiol 113:773–782.

Nowak L, Bregestovski P, Ascher P, Herbet A, Prochiantz A (1984) Magnesium gates glutamate-activated channels in mouse central neurones. Nature 307:462–465.

Okabe S, Collin C, Auerbach JM, Meiri N, Bengzon J, Kennedy MB, Segal M, McKay RD (1998) Hippocampal synaptic plasticity in mice overexpressing an embryonic subunit of the NMDA receptor. J Neurosci 18:4177–4188.

Panchenko VA, Glasser CR, Mayer ML (2001) Structural similarities between glutamate receptor channels and K^+ channels examined by scanning mutagenesis. J Gen Physiol 117:345–360.

Qian A, Antonov SM, Johnson JW (2002) Modulation by permeant ions of Mg^{2+} inhibition of NMDA-activated whole-cell currents in rat cortical neurons. J Physiol (Lond) 538:65–77.

Qian A, Buller AL, Johnson JW (2005) NR2 subunit-dependence of NMDA receptor channel block by external Mg^{2+}. J Physiol (Lond) 562:319–331.

Rose CR, Konnerth A (2001) NMDA receptor-mediated Na^+ signals in spines and dendrites. J Neurosci 21:4207–4214.

Shi N, Ye S, Alam A, Chen L, Jiang Y (2006) Atomic structure of a Na^+- and K^+-conducting channel. Nature 440:570–574.

Sigworth FJ, Sine SM (1987) Data transformations for improved display and fitting of single-channel dwell time histograms. Biophys J 52:1047–1054.

Spassova M, Lu Z (1998) Coupled ion movement underlies rectification in an inward-rectifier K^+ channel. J Gen Physiol 112:211–221.

Thompson CL, Drewery DL, Atkins HD, Stephenson FA, Chazot PL (2002) Immunohistochemical localization of *N*-methyl-D-aspartate receptor subunits in the adult murine hippocampal formation: evidence for a unique role of the NR2D subunit. Brain Res Mol Brain Res 102:55–61.

Tsuzuki K, Mochizuki S, Iino M, Mori H, Mishina M, Ozawa S (1994) Ion permeation properties of the cloned mouse epsilon 2/zeta 1 NMDA receptor channel. Brain Res Mol Brain Res 26:37–46.

Vargas-Caballero M, Robinson HP (2003) A slow fraction of Mg^{2+} unblock of NMDA receptors limits their contribution to spike generation in cortical pyramidal neurons. J Neurophysiol 89:2778–2783.

Wollmuth LP, Sobolevsky AI (2004) Structure and gating of the glutamate receptor ion channel. Trends Neurosci 27:321–328.

Woodhull AM (1973) Ionic blockage of sodium channels in nerve. J Gen Physiol 61:687–708.

Wyllie DJ, Behe P, Nassar M, Schoepfer R, Colquhoun D (1996) Single-channel currents from recombinant NMDA NR1a/NR2D receptors expressed in *Xenopus* oocytes. Proc R Soc Lond B Biol Sci 263:1079–1086.

Wyllie DJ, Behe P, Colquhoun D (1998) Single-channel activations and concentration jumps: comparison of recombinant NR1a/NR2A and NR1a/NR2D NMDA receptors. J Physiol (Lond) 510:1–18.

Zhang L, Rzigalinski BA, Ellis EF, Satin LS (1996) Reduction of voltage-dependent Mg^{2+} blockade of NMDA current in mechanically injured neurons. Science 274:1921–1923.

Zhong J, Russell SL, Pritchett DB, Molinoff PB, Williams K (1994) Expression of mRNAs encoding subunits of the *N*-methyl-D-aspartate receptor in cultured cortical neurons. Mol Pharmacol 45:846–853.

Zhu Y, Auerbach A (2001a) Na^+ occupancy and Mg^{2+} block of the *N*-methyl-D-aspartate receptor channel. J Gen Physiol 117:275–286.

Zhu Y, Auerbach A (2001b) K^+ occupancy of the *N*-methyl-D-aspartate receptor channel probed by Mg^{2+} block. J Gen Physiol 117:287–298.